14

Metal Oxide ZnO-Based Varistor Ceramics

Mohammad Reza Meshkatoddini
Faculty Member of Shahid Abbaspour PWUT University of Technology (SAUT), Tehran, Iran

1. Introduction

The metal oxide ZnO-based varistors are non-linear ceramic resistors which are largely used to protect the electric and electronic circuits and components against overvoltages. These varistors, which are among the most non-linear discovered materials, are used in lightning arresters owing to their strongly non-linear characteristics I(V). (Figure 1).

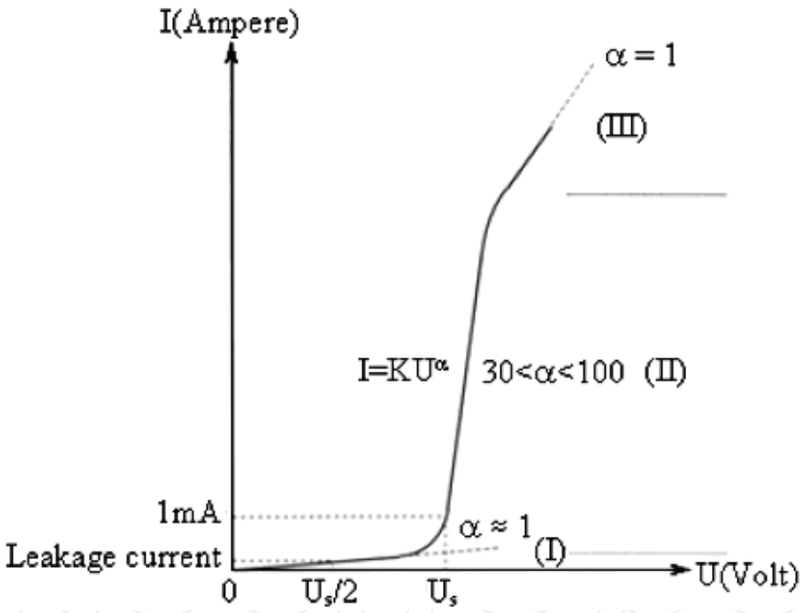

Fig. 1. Current versus Voltage characteristic in a ZnO-Based Varistor.

A varistor is a type of resistor with a significantly non-ohmic current-voltage characteristic. The name is a portmanteau of variable resistor, which is misleading since it is not continuously user-variable like a potentiometer or rheostat and is capacitor rather than resistor at low field. The most famous type of varistor is metal oxide varistor (MOV), which is also called as ZnO varistor. These varistors are used to protect circuits against excessive voltages. They have become more and more important during the past four decades due to their highly non-linear electrical characteristics and their large energy absorption capacity. They are normally connected in parallel with an electric device to protect it against the overvoltages. They contain a mass of zinc oxide grains in a matrix of other metal oxides

sandwiched between two plasma sprayed metal electrodes. The ZnO grains have dimensions in the range of 10μm to 100μm. The boundaries between the grains form double potential barriers with Schottky junctions having conduction voltages in the range of 3.5V. The boundary between each grain and its neighbor forms a Zener-like diode junction. ZnO grains are separated by these "active" grain boundaries of nanometers thickness. Then the mass of randomly oriented grains is electrically equivalent to a network of back-to-back diode pairs, each pair in parallel with many other pairs. When a small or moderate voltage is applied across the electrodes, a small thermally activated reverse leakage current flows through the diode junctions. When a large voltage is applied, the diode junctions break down from the avalanche effect, and large current flows. The result of this behavior is a highly nonlinear current-voltage characteristic, in which the MOV has a high resistance at low voltages and a low resistance at high voltages.

Three regions can be distinguished in the current voltage characteristics of the ZnO varistor. At low voltages, the insulating barriers between the grains result in a very high and almost Ohmic resistivity, which is called the pre-breakdown or Ohmic region. At a certain voltage, called the threshold or breakdown voltage, the system enters the breakdown region in which the current increases abruptly, and the dependence of current on voltage is described by the empirical relation:

$$I = k\, V^{\alpha} \tag{1}$$

From which the parameter α is equal to:

$$\alpha = d\,[\log(I)] \,/\, d\,[\log(V)] \tag{2}$$

This parameter is a measure of the element nonlinearity, which varies with voltage. At higher current densities, the voltage starts to increase again resulting in an upturn region of the I-V characteristic. This voltage increase gradually becomes linear with current, i.e. Ohmic, and is associated with the resistivity of the ZnO grains, i.e. the voltage drop in the ZnO grains.

Among their electric properties the most important ones are:

- The threshold voltage: It can be defined as the value of the voltage across the varistor, corresponding to a current of 1mA passing through it. From this voltage value, the varistor starts to change from the insulating state into the conducting state.
- Energy capacity: It is the maximum capacity of the energy absorption of a varistor without any damage, while the discharge current due to an overvoltage passes through it.

The other properties (chemical, mechanical...) are closely related to the two properties quoted above.

We have tried in our works to accomplish several statistical studies on these varistors, to find suitable ways to control their main characteristics such as the nonlinearity coefficient and conduction threshold voltage.

These varistors are composed of zinc oxide and some other metal oxides, which provide the desired characteristics for these varistors. The microstructure of the varistor ceramics develops while sintering ZnO powder doped with small amounts of additives such as Bi_2O_3, Sb_2O_3, Mn_3O_4, Co_3O_4, Cr_2O_3 and others, at a temperature in the range of 1100 to 1300°C.

The typical microstructure of a ZnO-based varistor is shown in figures 2 and 3. It is composed of ZnO matrix grains doped with Co, Mn, and Ni. These grains are n-type semi-

conductors. Both Bi_2O_3-rich and $Zn_7Sb_2O_{12}$ spinel phases are also usually present at the grain boundaries of the ZnO, but the presence of a $Bi_3Zn_2Sb_3O_{14}$ phase is possible as well. ZnO-ZnO grain boundary, rich of Bismuth, which is a highly resistive phase, is the main cause of the varistor effect, while spinel-ZnO junctions do not contribute to the nonlinear effect.

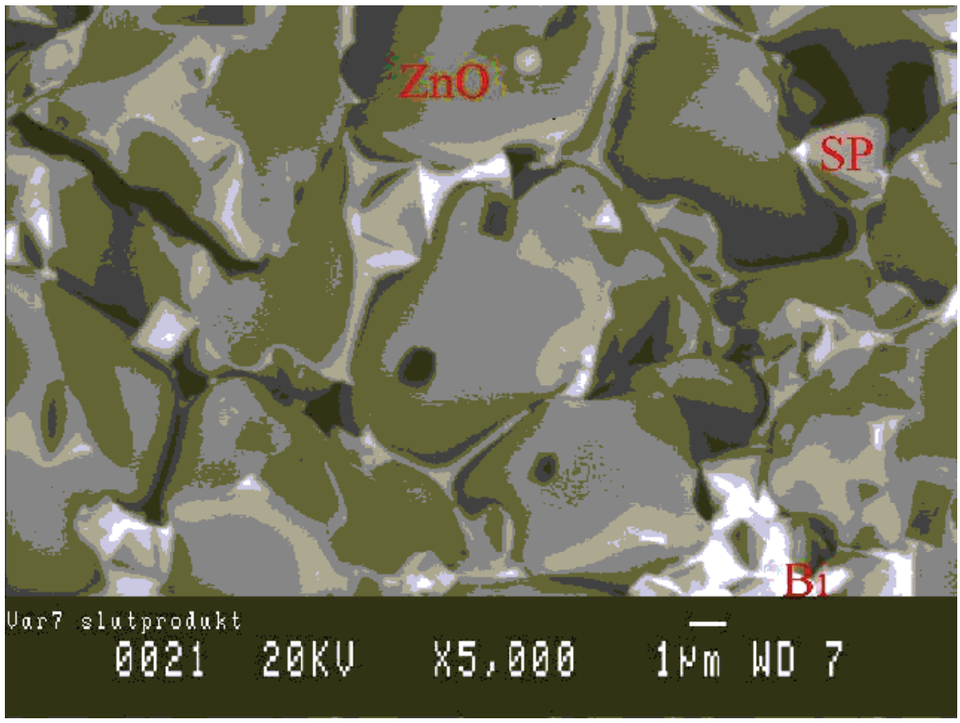

Fig. 2. Typical microstructure of a ZnO varistor taken by electronic microscope. (ZnO=Zinc oxide grain, Bi=Bismuth, Sp=Spinel phase).

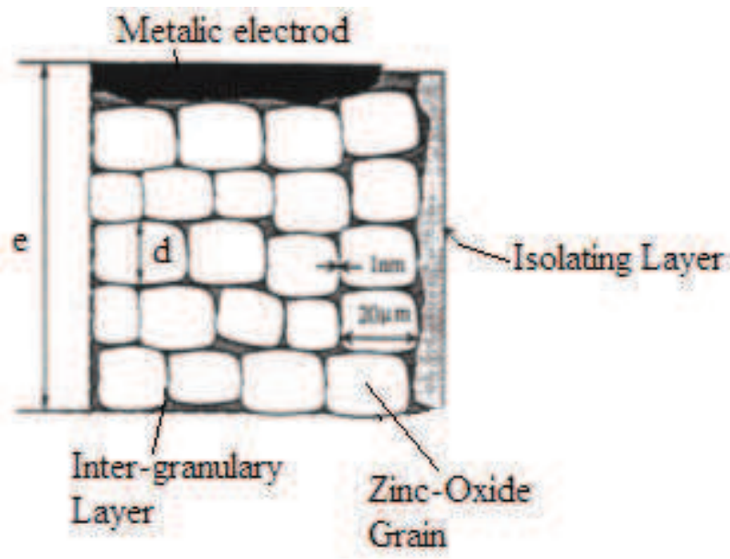

Fig. 3. A Model of ZnO-ZnO grain boundaries in a zinc oxide varistor.

The size of ZnO grains (d in Figure 2) determines the number of ZnO grain boundaries between the electrodes of the varistor. As mentioned before, the typical breakdown voltage for a non-ohmic ZnO-ZnO grain boundary is around 3 Volts, and hence, the size of the grains determines the overall breakdown voltage of varistor and then the length of the varistor column in a lightning arrester.

Sb_2O_3 is the standard additive for inhibiting the ZnO grain growth. The inhibition of ZnO grain growth is normally attributed to the existence of $Zn_7Sb_2O_{12}$ spinel-type particles, formed during heat treatment in ZnO grain boundaries.

To decrease dimensions of the varistors, and at the same time, to save the raw materials, many tests have been carried out on various formulations in order to apprehend an increase in the threshold electric field. There are many researches on this subject by adding additive oxides such as the lithium oxide, the magnesium oxide, the antimony oxide, etc. But one often runs up against the same difficulty; plus the threshold voltage is raised, plus the energy capacity decreases. For example when the threshold voltage is around 100V/mm, the capacity for energy absorption is in the order of 100 to 120 J/cm^3, but when the threshold voltage is about 350 V/mm, the capacity for absorption of energy falls down to 30 J/cm^3.

Another type of varistor has been proposed, which is made by adding a certain percentage of some rare earth oxides such as praseodymium, Pr_6O_{11}, to the traditional composition. The analysis of the results of the electric characteristics of the various studied samples has made it possible to highlight a threshold voltage of about 300 to 400 V/mm, and a capacity for absorption of energy about 90 to 120 J/cm^3. The increase in the height of potential barrier and the inhibition of the growth of the grains during the sintering cycle explain this physical phenomenon.

For a high energy-absorption capacity, a micro-structural homogeneity (uniform ZnO grain-size distribution; uniform distribution of phases along the grain boundaries of ZnO; no or at least very little fine porosity) is required, that allows a uniform current and hence an energy distribution throughout the whole varistor.

2. Manufacturing of ZnO-based varistors

Normally the varistors are prepared by traditional method used for electro-ceramics (Figure 4).

The principal chemical formulation is made up of about 95% ZnO, plus Bi_2O_3, Sb_2O_3, Co_2O_3, MnO_2, Cr_2O_3 and NiO as additives. All these oxides are mixed in a plastic earthenware jar with balls with zirconium, and pure ion-free water distilled during 24 hours. Rare earth oxide (Pr_6O_{11} or Nd_2O_3) can be added too in the principal composition. The powder is obtained after drying and 150μm sifting. An appropriate dimension of the blocks to be made and tested in an experimental procedure can be 26mm in diameter and 2mm of thickness, but industrial varistors have much bigger dimensions, up to tens of centimeters as diameter and height. They are sintered during a period in the range of 2 hours. Electrodes are deposited on two surfaces of the samples to provide electric connections and to measure I(V) characteristics. These characteristics are measured while continuous currents up to 10mA pass through the samples, and impulses of great amplitude by using 4/10 and 8/20μs impulse generators up to tens of kA are applied.

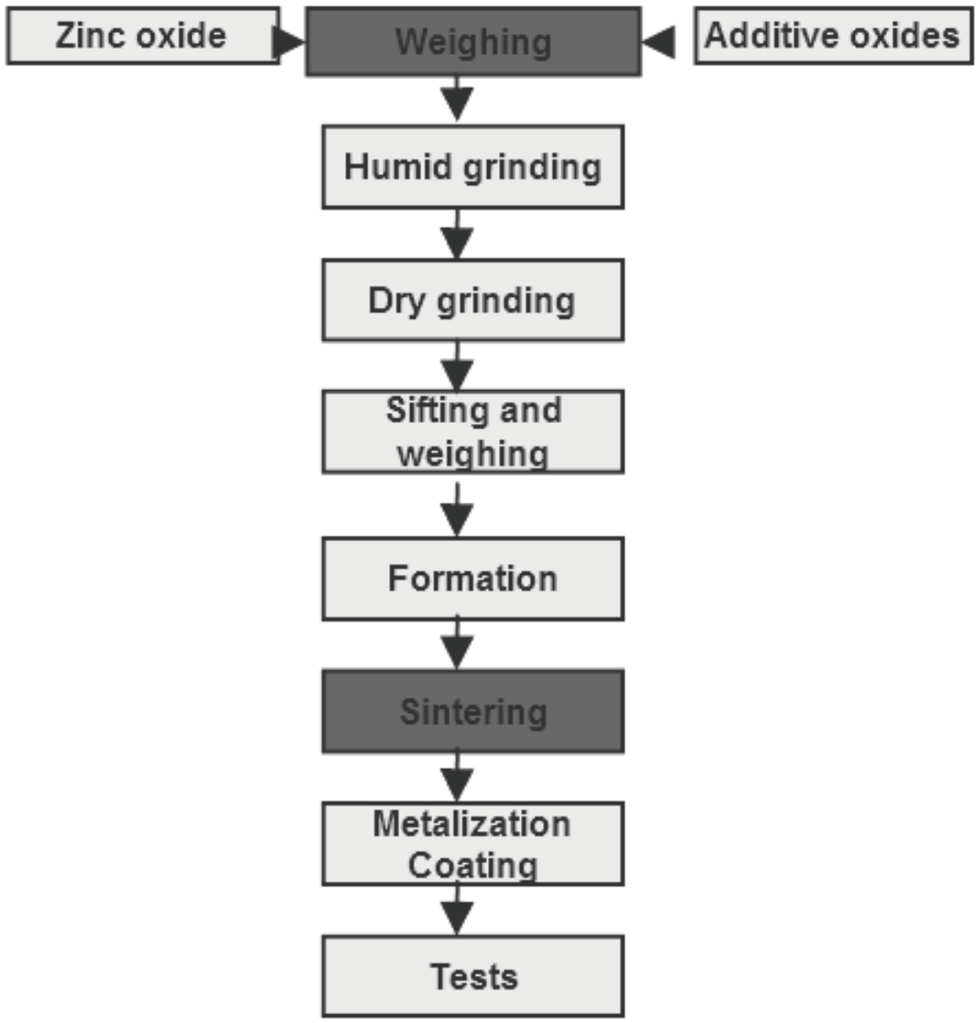

Fig. 4. Traditional procedure to manufacture a ZnO-based varistor.

Some examples for experimental composition of the samples are given in Table I. The composition S_1 can be modified by the addition of small amounts of Pr_6O_{11} or Nd_2O_3 to obtain the compositions S_2 and S_3, respectively.

Sample	Composition
S_1	95.0 % ZnO + 2.5 % Sb_2O_3 + 0.5% Co_3O_4 + 0.5%Cr_2O_3 + 0.5 % MnO_2 + 0.5 % NiO + 0.5 % Bi_2O_3
S_2	99.9 % S_1 + 0.1 % Pr_6O_{11}
S_3	99.9 % S_1 + 0.1 % Nd_2O_3

Table I. Some experimental compositions of ZnO varistor samples.

Reagent-grade oxides are mixed in appropriate ratios for each composition, and disks are cold pressed at a pressure up to hundreds of MPa. Electrodes are coated on parallel surfaces of the sintered samples. Polished cross sections of the samples are prepared, and the microstructures of the samples are examined using Scanning Electron Microscope (SEM).

3. Measurement of electrical properties

The current versus voltage (I-V) characteristics of the varistor samples are measured using a dc power supply up to tens of mA, and a 4/10μs impulse generator up to 100 kA, to identify the upturn voltage and the current energy absorption capacity. Energy-absorption capacity (A) is the maximum amount of lightning energy absorbed and/or passed through a varistor when it explodes. To measure this capacity, impulse currents are applied to the samples with increasingly larger amplitudes.
The current I(t) and the voltage V(t) waveforms are recorded with a storage oscilloscope. The energy absorption is calculated as follows.

$$A = I(t)\, V(t)\, dt \tag{3}$$

This parameter is calculated for all samples, and the average energy absorption is used to estimate the result. As an example, the electrical properties of some experimental varistor samples are given in Table II. As can be observed, the introduction of small amounts of rare earth oxides (REO) into composition S_1, with a threshold voltage (V_{1mA}) of 280V/mm, increased the threshold voltage of sample S_2, doped with Pr_6O_{11}, and sample S_3, doped with Nd_2O_3, to slightly above 300 V/mm. But what is more significant, is that doping with REO strongly increased the energy absorption capacity of samples S_2 and S_3 in comparison with sample S_1, from 52 to 112 J/ cm^3.

Sample	α	V_{1mA} (V/mm)	V_{GB} (V)	A J/cm^3
S_1	42	280	1.9	52
S_2	40	312	1.5	107
S_3	52	302	2.5	112

Nonlinear coefficient (α), Threshold voltage (V_{1mA}), Breakdown voltage per grain boundary (V_{GB}), and Energy absorption capacity (A) of varistor samples.

Table II. Average Current-Voltage characteristics

Further investigation shows that when the Pr_6O_{11} content increases, the threshold voltage increases as well but the coefficient of non-linearity α decreases.

4. Study of the varistors' microstructure

The microstructures of some investigated samples are presented in Figure 5. Phase composition and the distribution of phases in samples S_1, S_2, and S_3 are evident from

micrographs 5(a) to 5(f). The analyses confirms presence of the $Zn_7Sb_2O_{12}$ spinel-type phase containing Cr, Mn, Co, and Ni and also Bi_2O_3-rich phases with Zn, Sb, Cr, Mn, Co, and Ni detected at the ZnO grain boundaries of all the samples.

We can also see that the Bi_2O_3-rich phase, although present in all samples and more noticeable in sample S_3. The analysis also confirms the presence of the $Bi_3Zn_2Sb_3O_{14}$ (called as pyrochlore-type phase), at the grain boundaries of ZnO in sample S_1. In samples S_2 and S_3, a new phase is determined containing oxides of Pr and Nd, respectively.

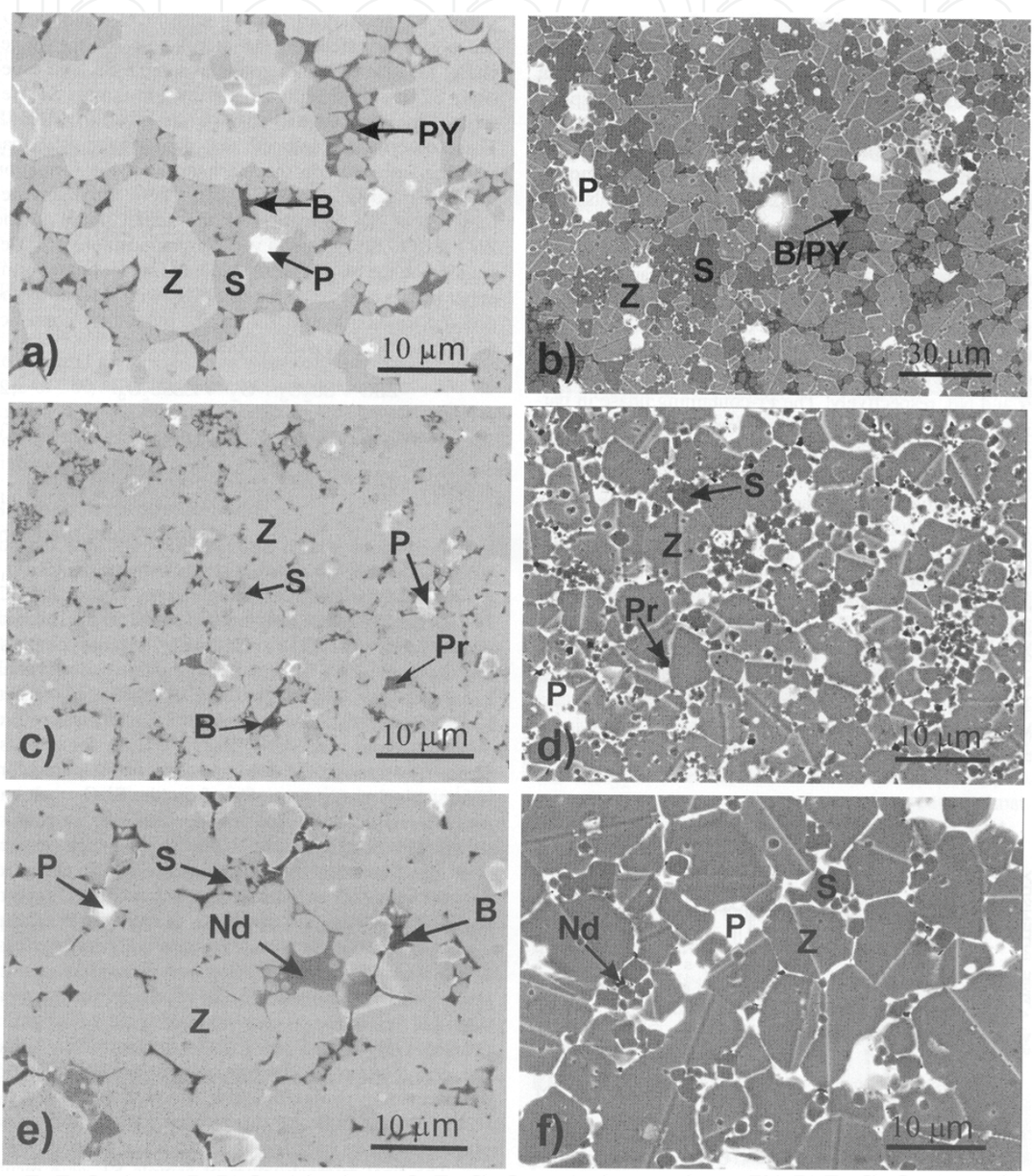

Key: Z=ZnO phase; B=Bi_2O_3-rich phase; S=$Zn_7Sb_2O_{12}$ spinel-type phase; PY=$Bi_3Zn_2Sb_3O_{14}$ (pyrochlore-type) phase; Pr=Pr-containing phase; Nd=Nd-containing phase; P=pore.

Fig. 5. Images from SEM of microstructures of varistor samples sintered at 1200^0C: (a) S_1; (b)S_1(etched), (c) S_2; (d) S_2(etched); (e) S_3; (f) S_3(etched).

The Pr-containing phase in particular is relatively fine-grained and distributed everywhere along the grain boundaries of the ZnO, while the grains of Nd-containing phase are larger and localized. While the grains of spinel phase are large in sample S_1, they are significantly smaller in samples S_2 and S_3. The formation of significant spinels in compositions with large amounts of added Sb_2O_3 has been observed by different researchers.
Thus micro-structural observations show a strong influence of REO doping on the ZnO and spinel grains, which is clearly evident from the micrographs in Figure 5. Doping of the composition with Pr_6O_{11} results in a significant decrease in the ZnO grain size and doping with both Pr_6O_{11} and Nd_2O_3 has a similar effect on the spinel phase; the size of spinel grains. Average size of the different phases of the varistor specimens are given in Table III.

Sample	ZnO		Spinel		Pores	
	D(μm)	δ (μm)	D(μm)	δ (μm)	D(μm)	δ (μm)
S_1	6.7	2.9	2.1	1.5	6.3	5.9
S_2	4.7	1.9	0.7	0.4	2.1	0.9
S_3	8.3	3.6	1.3	0.7	3.6	2.0

Table III. Average size D (μm) of ZnO grains, spinel grains, and pores of varistor samples S_1, S_2, and S_3 with corresponding deviations δ (μm).

These observations indicate that doping with REO has a strong influence on the mechanism of formation of the $Zn_7Sb_2O_{12}$ spinel phase. There are many reports in the literature about the formation of the spinel phase in the ZnO-Bi_2O_3-Sb_2O_3-based varistor compositions. Depending on the Sb_2O_3 / Bi_2O_3 ratio, the spinel phase forms either by the direct reaction of Sb_2O_3 with ZnO or by the decomposition of the $Bi_3Zn_2Sb_3O_{14}$ (named as pyrochlore phase) according to the following reactions:

$$ZnO + Sb_2O_3 + O2 \text{ ----> } ZnSb_2O_6 \quad (4)$$

$$ZnSb_2O_6 + 6\ ZnO \text{ ---> } Zn_7Sb_2O_{12} \quad (5)$$

$$2\ Bi_3Zn_2Sb_3O_{14} + 17\ ZnO \text{ ---> } 3\ Zn_7Sb_2O_{12} + 3\ Bi_2O_3 \quad (6)$$

The increase in threshold voltage (V_{1mA}) can be ascribed to the smaller ZnO grain size. However, the increase in V_{1mA} is much smaller than could be expected from the large decrease in the ZnO grain size and suggests that the increase in the number of non-ohmic grain boundaries is not proportional to the increase of all ZnO-ZnO grain boundaries due to the smaller ZnO grain size in this sample. It is evident from Table II that the average breakdown voltage of the grain boundary (V_{GB}) in sample S_1 is 1.9 V, while in sample S_2 it is only 1.5 V. Sample S_3 also has a significantly higher V_{1mA} than sample S_1, despite the fact that it has a larger ZnO grain size than sample S_1. The V_{GB} in sample S_3 is 2.5 V which indicates that a larger fraction of grain boundaries in this sample has a non-ohmic character.

Sample S_3 also has a higher nonlinear coefficient α of 52 than samples S_1 and S_2 with α equal to 40.

Doping with REO significantly improves the energy characteristics of samples. The low energy-absorption capacity of sample S_1 can be attributed to the large amount of spinel phase in this sample.

The spinel phase forms large grains along the grain boundaries of ZnO, and so insulating chains of spinel phase significantly interrupt the current flow by narrowing the effective conduction section of the varistor. This leads to current localization and local overload, and hence a low energy-absorption capacity due to a non-uniform energy distribution.

The analysis of the whole results obtained during the tests of the samples, manufactured with various percentages of praseodymium and neodymium oxides makes it possible to suggest that:

- The presence of rare earth oxides improves the homogenization of the size of the grains in material.
- The increase of potential barrier height in the grain boundary supports a rise in the threshold electric field of the varistor.
- A good capacity of energy absorption is resulted compared to the traditional varistors.

Doping with Pr_6O_{11} and Nd_2O_3 appears to be promising for the preparation of ZnO-based varistors with a high breakdown voltage and also high energy-absorption capacity. This can be a successful step because our objective is to have smaller and lighter surge arresters in power network. This aim involves such varistors, which have high conduction threshold voltage, while their energy absorption capacity remains enough high. In such conditions we will be able to use a smaller number of varistors to make a high-voltage arrester. Consequently this will provide smaller and lighter arresters.

Of course we have to respect the necessary outer creepage distance of the arrester housing, according to the pollution level of the location where the arrester is to be used.

5. Computation of nonlinear properties in ZnO ceramics

Different computational methods are used for investigation of the non-linear behaviour of zinc-oxide varistors. In a ZnO varistor, when a voltage is applied between the electrodes, the majority of the grain boundaries show a strong non-linear behavior, but a certain number of grains do not present, under the applied voltage, a high non-linear characteristic or are nonconducting. Under a known voltage level, several current paths occur from one electrode to the other, which are called as the current percolation paths. The number of grains on each path crossing by the current is a statistical parameter. It is shown that the distribution of this statistical number depend on the block thickness and percentage of nonconducting grains in the varistor.

Using a Monte Carlo method in our research works, we have realized that the number of ZnO grains providing the percolation path fits a lognormal distribution especially in thin varistors. We have also proposed a binomial direct approach for this problem. It is found that the direct approach could be satisfying too.

Both approaches show that the threshold voltage and the nonlinearity coefficient of the varistors can be controlled, to some degree, by the fraction of nonconducting grains. These results help us to have a better understanding of the varistors' behavior and enable us to make more realistic electric models for these elements.

Few works can be found, which have experimentally studied the individual grain boundaries in the varistor. Most of the Schottky junctions give a nonlinearity coefficient which is normally in the range of 30-70 for a normal varistor, whereas the actual α of a good ZnO material junction can be in the range of 150. Even it can attain values greater than 200 in certain grain to grain microvaristors. Figure 6 shows the typical variation of the current density as a function of the barrier voltage, for a single barrier in a varistor.

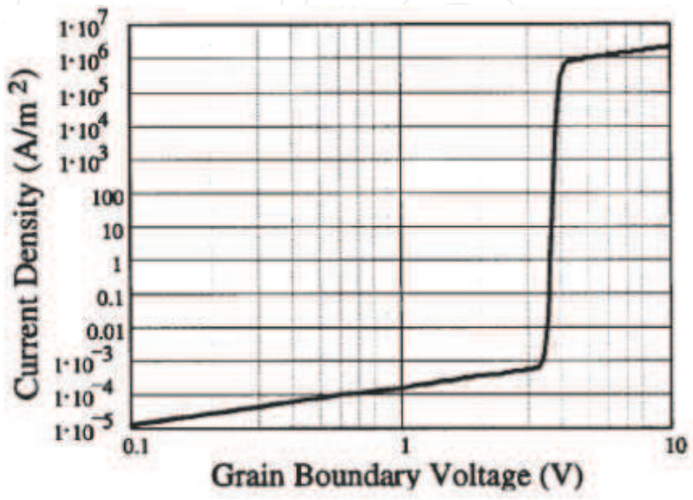

Fig. 6. The grain boundary current density vs. grain boundary voltage.

In Figure 7 the variation of the non-linearity coefficient α as a function of the varistor barrier voltage, for a single potential barrier is observed. This curve is deduced computationally, using Maple software, from the slope of the current-voltage characteristic of a single grain boundary as in Figure 6.

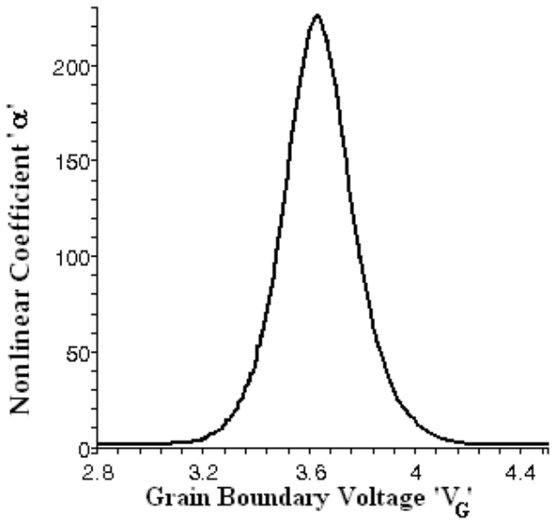

Fig. 7. Non-linearity coefficient α as a function of the varistor barrier voltage, for a single potential barrier.

5.1 Model of the varistor's microstructure

In Figure 8 a simplified model of the varistor's microstructure is observed. We use this model for computer simulation.

If the ZnO element thickness is D and the average grain thickness is d, then the minimum number of grain boundaries between the electrodes is L=D/d.

5.2 Monte Carlo method

As we read in the literature, the Monte Carlo is a technique that provides approximate solutions to problems expressed mathematically. Using random numbers and trial and error, it repeatedly calculates the equations to arrive at a solution. Then using random numbers or more often pseudo-random numbers, as opposed to deterministic algorithms, uses this algorithm for solving various kinds of computational problems.

Monte Carlo methods are extremely important in computational physics and related applied fields. Interestingly, the Monte Carlo method does not require truly random numbers to be useful. Much of the most useful techniques use deterministic, pseudo-random sequences, making it easy to test and re-run simulations. The only quality usually necessary to make good simulations is for the pseudo-random sequence to appear "random enough" in a certain sense. They must either be uniformly distributed or follow another desired distribution when a large enough number of elements of the sequence are considered. Because of the repetition of algorithms and the large number of calculations involved, Monte Carlo is a method suited to calculation using a computer, utilizing many techniques of computer simulation.

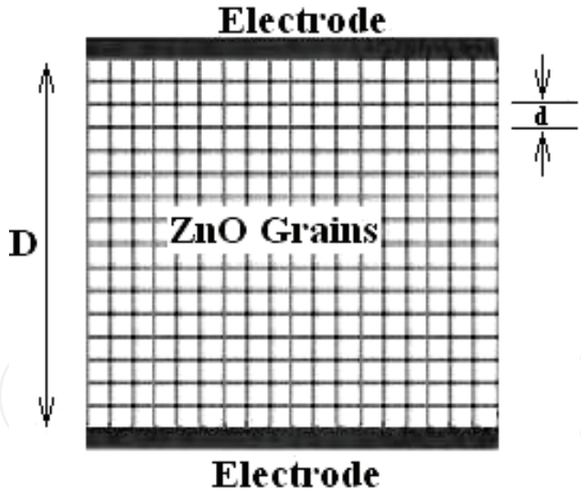

Fig. 8. Simplified micro-structural model of varistor for computer simulation.

Using a Monte Carlo algorithm, we follow a stochastic procedure to compute the number of the conducting grains on the current path in the varistor model as a statistical parameter. The flowchart of the used program is observed in Figure 9. In this diagram the letters K and N denote, respectively, the iteration number and the variable for the number of each layer in micro-structural model of the varistor. B is the number of active grain boundaries through which the current passes in going from one electrode to the other. As well, we define the probability of a non-conducting grain boundary as P. For P=0, all grain boundaries are

always active. It is obvious that the existence of non-conducting grains results in a longer path for current across the ZnO element, which depends on the fraction of non-conducting grains. We undertake a statistical analysis of the effect of L (the number of ZnO grain layers across the varistor) and P (the probability of a non-conducting grain boundary) on the non-linear characteristics of the varistor as characterized by α.

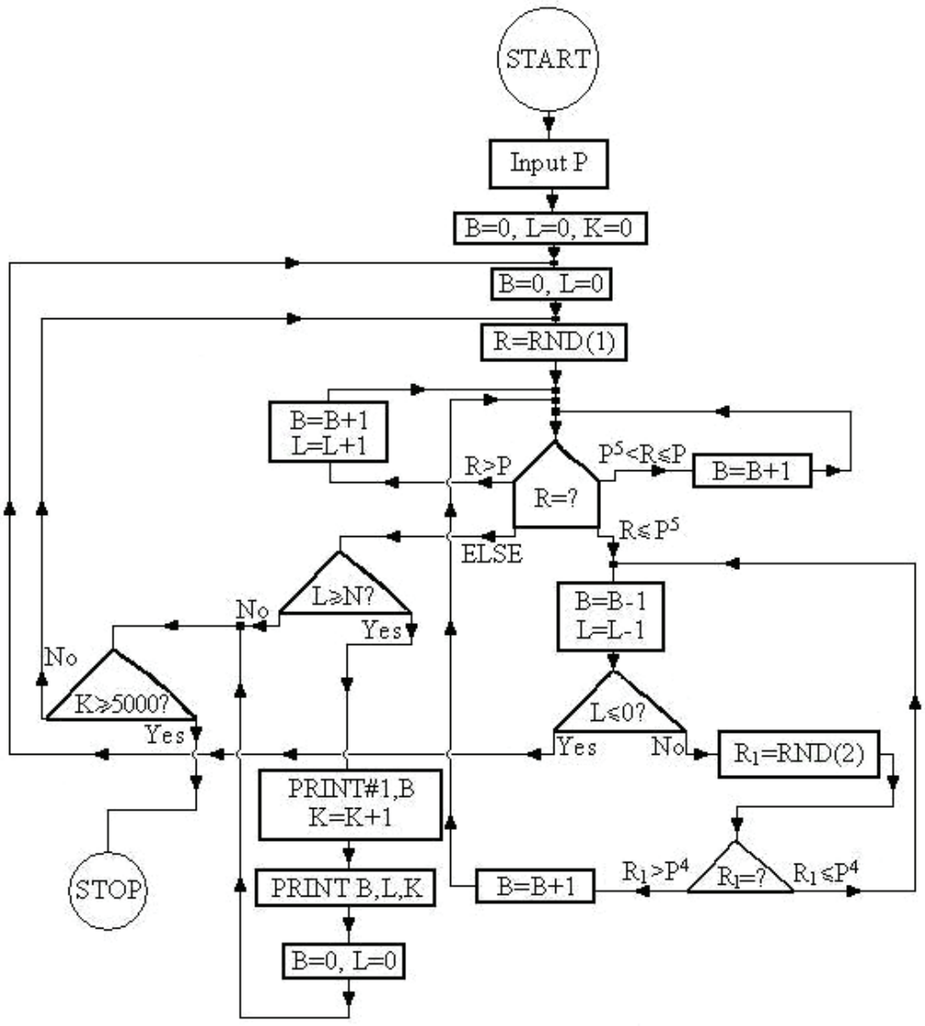

Fig. 9. Flowchart of Monte Carlo algorithm, for computation of the number of grains on the current path through the varistor.

As said above, for P=0, there is no non-conducting grains and all path lengths are the same, equal to L. With increasing fraction of non-conducting grain boundaries P, the conducting grains number B, augments substantially, which will increase the voltage per unit thickness of the ZnO element. P can also be augmented by increasing the amount of non-conducting inter-grain material, often as a by-product of attempting to reduce grain size. This non-conducting phase can be a spinel phase. Obviously increasing the number of non-conducting grain boundaries increases the current density in the remaining grain boundaries and results in greater grain boundary power dissipation and temperature rise.

By running the Monte Carlo program with different values of L, the number of ZnO grain layers across the varistor, and P, the probability of non-conducting grain boundaries in varistor, we obtain statistical sets of data for B, i.e. the number of grains crossed by the current.
As an example, a probability density histogram of B's data for the case of a very thin varistor with L=10 and P=0.3 is seen in Figure 10, which is related to a varistor of about 0.1 mm thick.

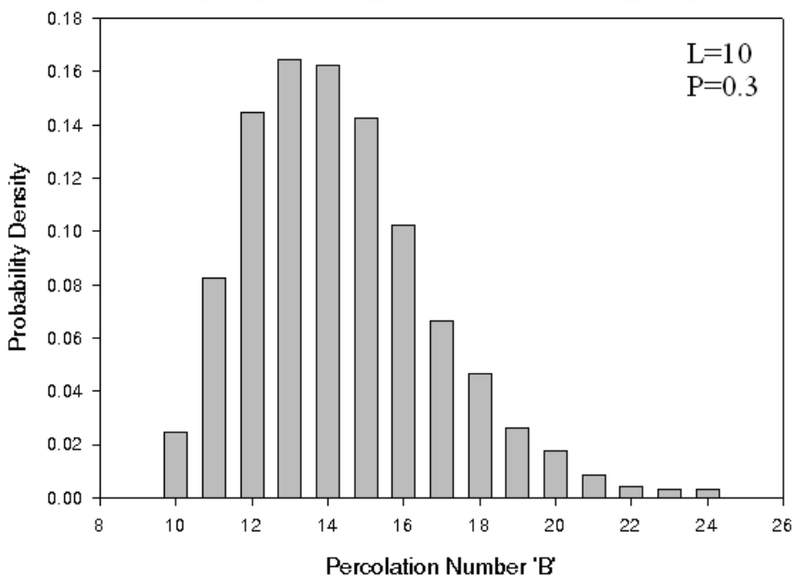

Fig. 10. A probability density histogram of the number of grains crossed by the current, obtained for special case of a very thin varistor of about 0.1 mm thick with probability of non-conducting grains equal to 30%.

Analyzing the statistical distribution of B by fitting different distribution curves on it, several distributions such as Normal, Lognormal, Weibull, Logistic, Loglogistic and Exponential were used for fitting our computational data. The best fitness was seen to be for the three distributions of Normal, Weibull and Lognormal (identically for Log_eNormal and Log_{10}Normal), comparing to the others.
In Figure 11 we can observe the fitted curves for these three distributions concerning the special case of Figure 10.
The Anderson-Darling statistic is a measure of how far the plot points fall from the fitted line in a probability plot. Using the Anderson-Darling measure to calculate the fit goodness of these distributions, we obtain the curves of Figure 12.
The statistic is a weighted squared distance from the plot points to the fitted line with larger weights in the tails of the distribution. In this method, a smaller Anderson-Darling (AD) measure indicates that the distribution fits the data better.
As can be observed in Figure 12, the LogNormal distribution has the best fit for the B data concerning the thin varistors of this study.
If the probability of a grain boundary to be non-conducting is P and as we supposed in our model that the grains are cubes, then it can be shown that to a first approximation, the mean number of active grain boundaries through which the current passes between electrodes is:

$$B = L\ (1 + \frac{P}{1\text{-}P}) \qquad 0 < P < 1 \tag{7}$$

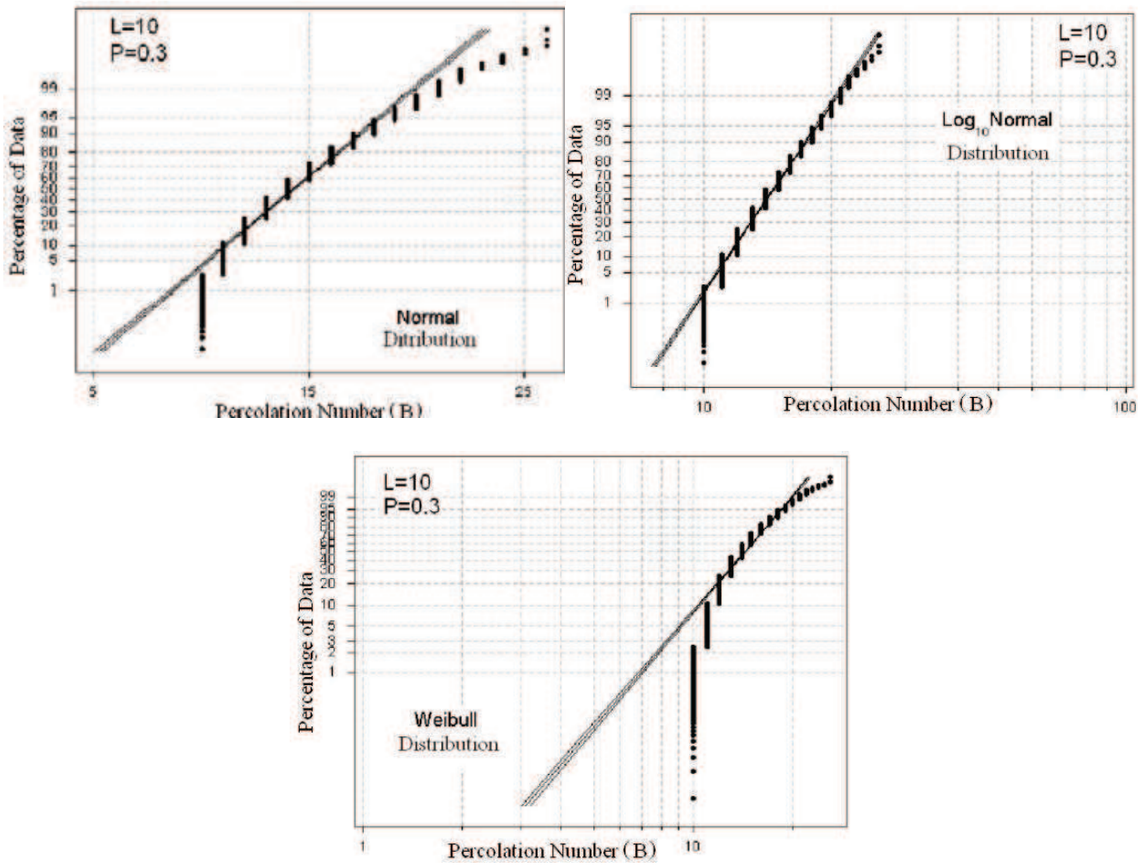

Fig. 11. Curve fitting of the number of grains crossed by the current, on three different distributions for the data of Figure 10.

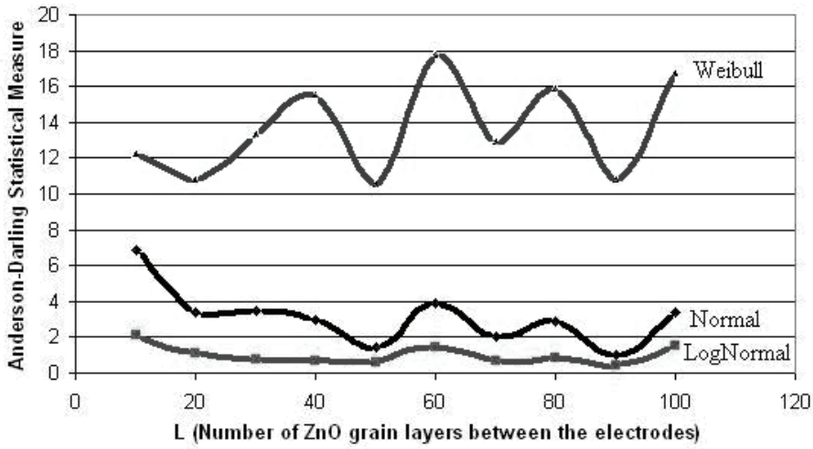

Fig. 12. Comparing the fitness of three different distributions on our data, concerning varistors of 0.1 to 1 mm thick.

And as we realized in our research work that the percolation number data for thin varistors obey the lognormal distribution, we deduce, using the Maple software, the relation (8) as an analytical formula for the standard deviation, s, of thin varistors data, having the lognormal distribution.

$$s := \sqrt{\left(e\right)^{\left(\frac{\left(\ln\left(L\left(1-\frac{P}{P-1}\right)\right)-\frac{\ln\left(L\left(1-\frac{P}{P-1}\right)\right)}{L}\right)^2}{L}\right)\left(\left(e\right)^{\left(\frac{\left(\ln\left(L\left(1-\frac{P}{P-1}\right)\right)-\frac{\ln\left(L\left(1-\frac{P}{P-1}\right)\right)}{L}\right)^2}{L}\right)}-1\right)} \quad (8)$$

By plotting this equation for different values of L and P in Maple software, we obtain Figure 13. As it is seen, the standard deviation is not high for amounts of P less than 0.5, while it is great for bigger P's in thinner varistor blocks.

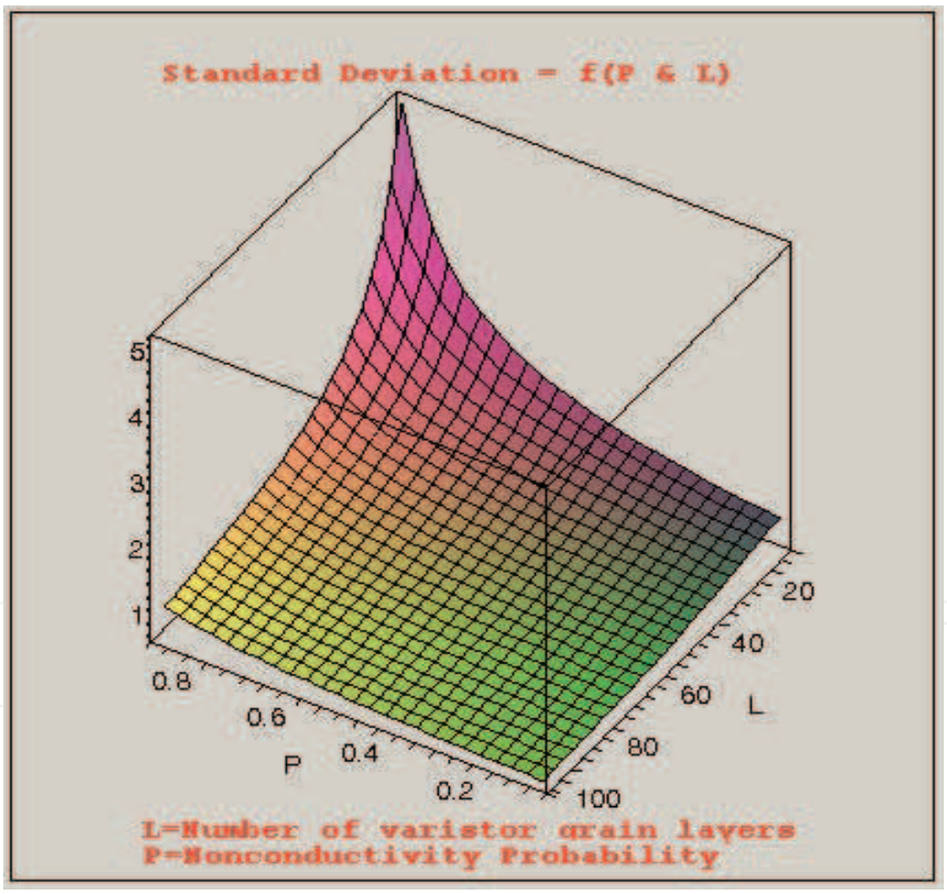

Fig. 13. Standard Deviation for percolation number B of thin varistors, having lognormal distribution.

We assumed that each current path is independent of every other path. In fact, at large P, the number of non-conducting grain boundaries would reduce the likelihood of

interconnection of paths. But in P less than 0.5, especially in thin varistors even if two paths of differing length are near each other, the probability of their having substantially differing potentials is not great.

We realize from the form of the statistical distribution for B, that as P increases, the varistor conduction turn-on will be more rapid. This can be deduced from the low B tail of the statistical distribution. For small L, the average value of B increases with P, but the minimum value of B, which is L, remains the same. Thus the ratio of the mean to minimum possible value of B increases. The turn-on characteristics are determined mainly by the first few paths to conduct. Thus the number or fraction of completed paths for various P must be considered in addition to α.

Figure 14 compares lognormal and Normal distributions with the same mean (200) and with variances selected to give the same minimum value (~100) in a population of 600 random numbers. This figure indicates that the probability density of B increases much more rapidly at low values of B for the lognormal than for the Normal distribution. Thus conditions, which drive the statistical distribution for B toward the lognormal distribution, are likely to result in more rapid turn-on of the varistor element. The lognormal distribution also has a long tail at high values, which will cause a long tail in α.

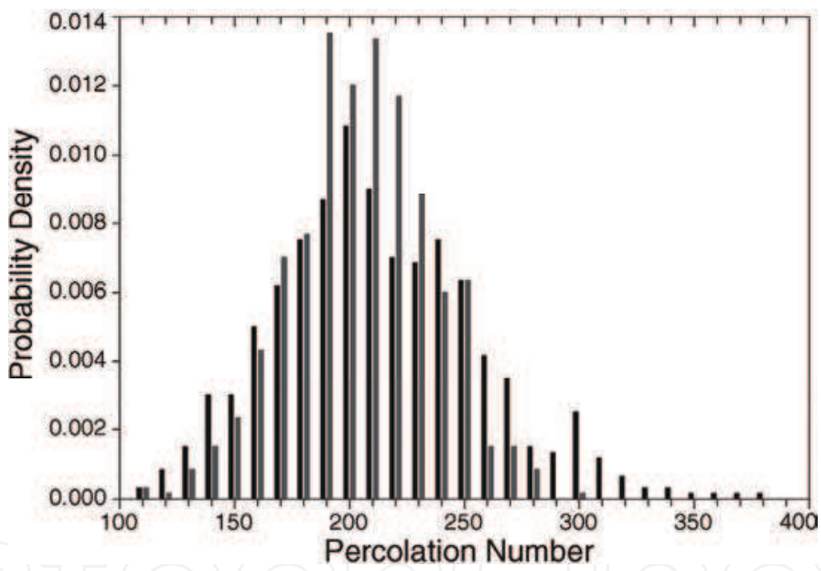

Fig. 14. Comparison of Lognormal (black) and Normal distribution data with same mean (200) and with variances set to give about the same minimum value (100) in a population of 600.

Based on the numerical computations and the distributions thereof, we believe that the more rapid turn-on as a function of increased P for large L (thick elements) is probably associated with a transition from a Normal distribution at P=0 toward a lognormal distribution with increasing P.

This transition can be rationalized from the probability density of B for a thin varistor with a reasonable probability of non-conducting grains, for which the distribution is clearly asymmetric with a rapid turn-on, when the shortest path across the arrester becomes conducting, followed by a rapid increase in the number of conducting paths with increasing voltage.

The Lognormal distribution increases more rapidly in the low end tail of the distribution which would result in a more rapid turn-on of an arrester element.
In Figure 15, the variation of α as a function of the applied voltage is seen for a non-conducting grain probability 0.5 for a thick varistor of 10 mm thickness (L=1000) and a thin varistor of 0.5 mm (L=50) thickness.
Both cases result in asymmetrical α characteristics, while the varistor thickness has an obvious influence on the shape of the curve. We accomplished the same analysis for varistors with different thickness (Number of grain layers L) and probability of non-conducting grains (P).

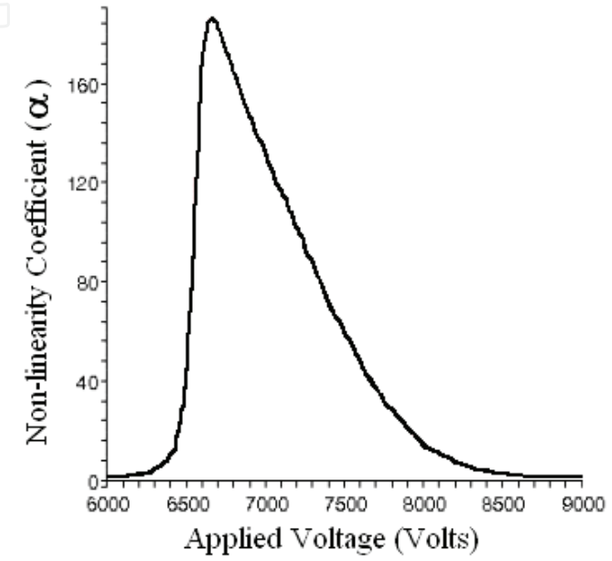

a) 10mm thick varistor (L=1000)

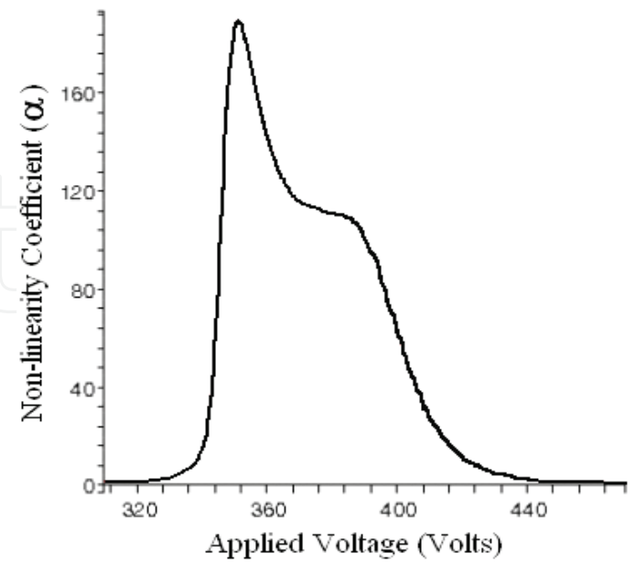

b) 0.5mm thick varistor (L=50)

Fig. 15. Varistor nonlinearity coefficient α as a function of the applied voltage for thin and thick varistors at a non-conducting grain probability of 0.5.

To provide a basis for comparison of the α(V) curves, we define the parameters FWHH and β as measures for broadness and rate of rise of the α(V) curve (Figure 16). We define FWHH as the Full Width at Half Height of the curve and β is defined as:

$$\beta = (V_{90\%} - V_{10\%}) / V_{10\%} \quad (9)$$

According to this definition for β, the small β means large slope of α(V) curve.
In Figure17, we see the variation of the (FWHH) of the α(V) curves as a function of L, which is linear as might be expected.

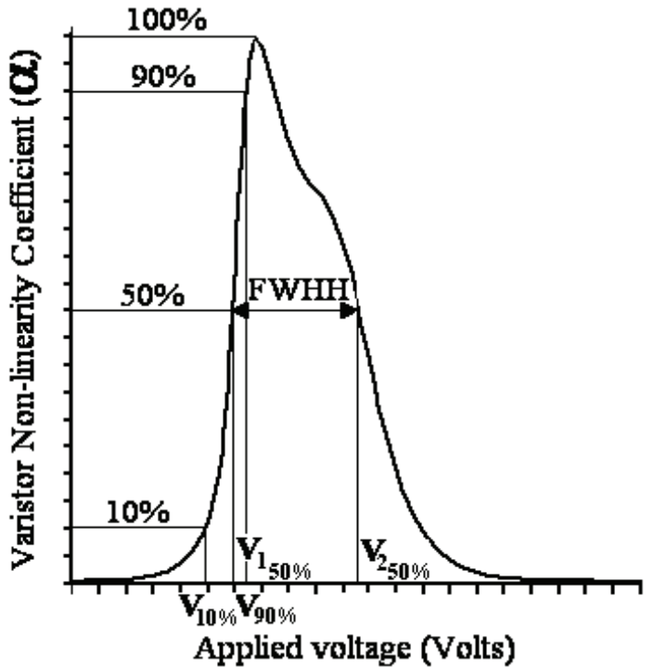

Fig. 16. Definition of parameters FWHH and β.

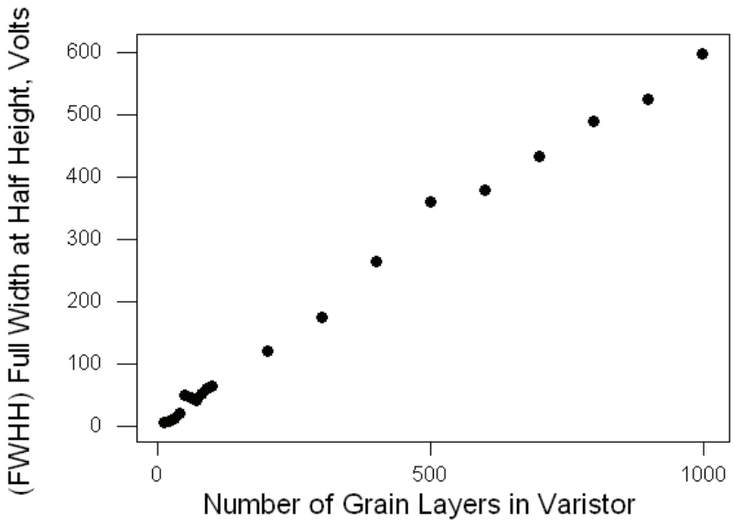

Fig. 17. Full Width at Half Height (FWHH) of the α(*V*) curves with P=0.5 as a function of L.

For P=0 and large L, the characteristics are just a multiple of the grain boundary characteristics which are modeled as symmetric. As the fraction of non-conducting grains increases, the mean percolation path increases and the probability of a short percolation path decreases.

However the minimum possible path remains the same (L) and above the minimum path, the number of conducting paths appears to increase rapidly which results in an asymmetric α with more rapid turn-on.

As both the threshold voltage and width of α are the sum of the contribution from each grain, i.e. a 10 mm thick varistor (L=1000) is equal to twenty 0.5 mm thick (L=50) varistors in series, so that the I(V) curve of the former will be sum of the I(V) curves of the latter. Thus FWHH(L) should increase linearly with L, and the result of Figure 16 can be taken as a verification of the computational methods.

Figure 18 shows the variation of β with non-conducting grain probability (P) for a thin (L=50) and a thick (L=1000) ZnO element. As we can see in this figure, the rate of rise of the α(V) curve depends on both the non-conducting grain probability and the element thickness.

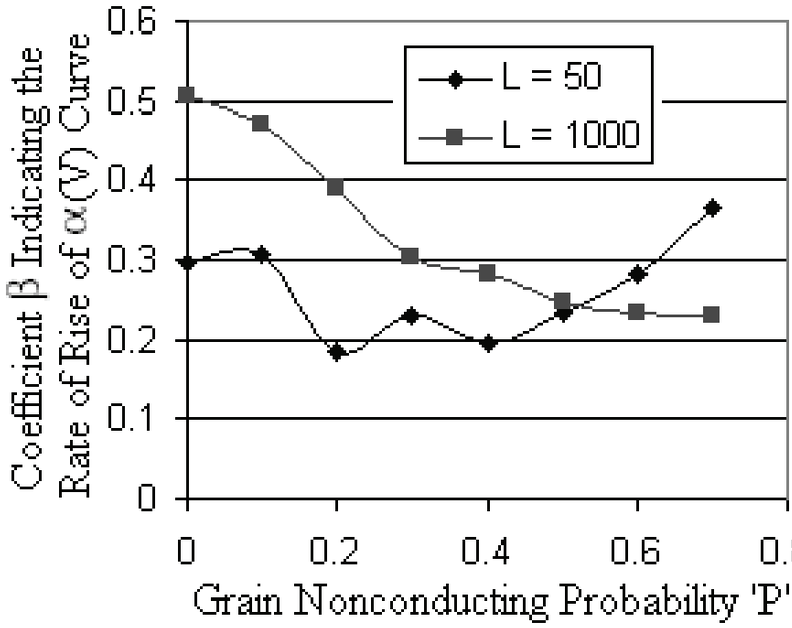

Fig. 18. Variation of β as a function of P, for L=50 (0.5 mm thick) and L=1000 (10 mm thick) varistors. Smaller β tends to indicate more rapid "turn-on" of the varistor with applied voltage.

For P>0.5 and large L (thick varistor), β remains constant, which means that increasing P has little effect on the varistor turn-on characteristics. This is probably a result of the fact that for large L, the standard deviation in B decreases as a fraction of L, so that the extreme value in B decreases relative to the mean.

With increasing P, the mean number of grain boundaries increases, as does the distribution of the number of grain boundaries through which the current passes from one electrode to the other. As the grain boundary characteristic is highly nonlinear, the conductivity of the

ZnO element rises rapidly once the first few current paths become conductive. This probably accounts for the increasing asymmetry in α for the whole varistor, and increasingly rapid current onset with increasing P, as the statistical distribution of path lengths broadens with P.

For large L, β decreases with increasing conducting grain probability, P, but for small L this is not the case. As well, the peak value of α increases with increased P for thick elements but not for thin elements. This must result from competition between the larger variance in B, the percolation path for small L, with the nature of the tail of the statistical distribution at low values of B, which determines the turn-on characteristics.

One would prefer the ZnO "turn on" (become substantially conductive) to be very rapidly so that the AC operating voltage can approach more closely the protection level of the varistor without causing excessive power dissipation. On the other hand, how the varistor approaches its ultimate conductivity with voltage is less important. As we observed, the probability, P, of non-conducting varistor grains has an influence on parameters such as the rate of rise of α(V) curve.

As a conclusion, we say that the characteristics of the thin ZnO varistors were statistically studied. The number of ZnO grains on each conducting path through a ZnO varistor, crossing by the current, is a statistical parameter (B).

It was shown that the nonlinearity of ZnO ceramics can be controlled, to some degree, by the fraction of non-conducting grains. Thus we can choose the best value for P to have the maximum rate of rise of the α(V) curve. This will result in a rapid "turn on" of the ZnO element, which allows the circuit being protected to operate more closely to the protection level without excessive power dissipation in the arrester element. This optimum value of P certainly depends L, which is related to the thickness of the varistor.

With increasing fraction of non-conducting grain boundaries P, the percolation number B, increases substantially, which will increase the voltage per unit thickness of the ZnO element. This can be exploited commercially in order to increase the percolation number.

These results can help us to have a better understanding of the behavior of these varistors, and the dependence of this behavior on their geometrical dimensions and the constituting materials. This will also enable us to have more realistic electric models for these ceramic elements.

5.3 Direct Binomial method

We propose also that the Binomial distribution can be used directly to explain the conduction phenomena in ZnO varistors. Here is a Maple program using the Binomial Distribution for computation of the current in the varistor and calculation of its α, to predict directly the turn-on characteristics. We use the Binomial Distribution formula to calculate the probability function of the L success in B trials (B=Percolation Number & L=Number of Layers).

For example we consider a varistor block with a diameter of 4cm (Dvaristor = 0.04).

Then we calculate the number of grains in the first layer, from which a current can be started, as follows:

$$\begin{gathered} S_{varistor} = \pi.(D_{varistor}^2) \,/\, 4 \\ D_{grain} = 0.000010 \\ S_{grain} = D_{grain}^2 \\ N_S = S_{varistor} \,/\, S_{grain} \end{gathered} \tag{10}$$

The number of the expected conducting grains just next to the upper electrode is:

$$N_P=N_S\ (1-P) \tag{11}$$

Now we compute the probability for the current to advance L layers in crossing B grains, from one electrode to the other, for a given L & P (in the example here L=100 and P=0.3):

$$F = (B!)\ /\ ((L!).(B-L)!) \tag{12}$$

$$\text{Probability}(L=100) = F\ .\ (((1-P)^{L}).(P^{(B-L)})); \tag{13}$$

Now we can have the number of current paths in the varistor as a function of B, i.e., we know that how many paths there are for each B:

$$N_B = (\text{Probability}(L=100))\ .\ N_P \tag{14}$$

Here we plot the number of the conduction paths, in a varistor with 100 layers and 30% of non-conducting grains, as a function of the percolation number B:

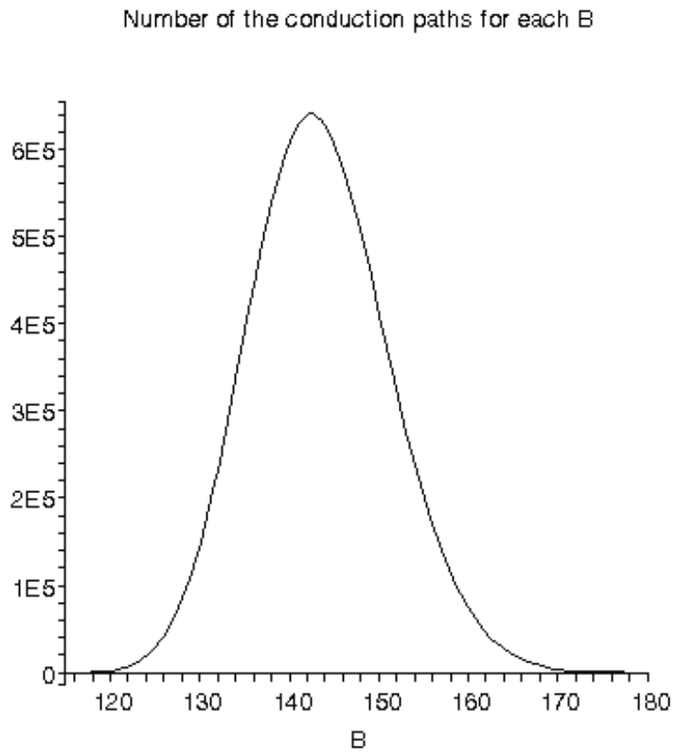

Fig. 19. Variation of P as a function of *B* for *L*=100 (~1 mm thick)

Now we compute the current per grain boundary, using the relation of $J(V_G)$ for one single grain boundary :

$$J = 10000\ 10^{[-4.5\tanh[-\frac{50\ \ln(VG)}{\ln(10)}+28]\ -5.5]}\ 10^{[\frac{10}{9}\frac{\ln(VG)}{\ln(10)}+\frac{20}{9}]} \quad (15)$$

Then we substitute VG by V/B, as the total voltage V which is applied on the whole varistor is distributed on B grains en series :

$$V_G = V/B \quad (16)$$

In L trials, the mean number of cases without a non-conducting grain is L(1-P) and the mean number with a non-conducting grain is L.P. We can ignore the cases, which are "dead ends", as they do not count:

$$L.(1-P) = B_M \quad (17)$$

Since these are the cases which move us forward. Thus for a probability of a non-conducting grain, P, the mean percolation number is:

$$B_M = N/(1-P) \quad (18)$$

B_M is the number of active grain boundaries through which the current passes between electrodes.

Now we compute the current flowing per each single path, from which the total current through the varistor can be obtained as follows:

$$I_B = J.S_{grain} \quad (19)$$

$$I_V = \Sigma(I_B.N_B\ , B=L \text{ to } 10L) \quad (20)$$

This is because the total current will be the sum of the number of paths multiplied by the current in each path. Using this second formula for calculating the current in whole range of B, the α will be obtained. We substitute V by V+1 in IV to obtain the derivative and calculate the Alpha as follows:

$$I_{V1} = subs(V=V+1,I_V) \quad (21)$$

$$\alpha = (\log_{10}(10^{-2}\ I_{V1})-(\log_{10}(10^{-2}\ I_V))) \ /(\log_{10}(V+1)-\log_{10}(V)); \quad (22)$$

From Figure 20, it is obvious that how asymmetric the α(V) curve is. For large L, β decreases with increasing conducting grain probability, P, but for small L this is not the case. As well the peak value of α increases with increased P for thick elements but not for thin elements. This must result from competition between the larger variance in B, the percolation path for small L, with the nature of the tail of the statistical distribution at low values of B, which determines the turn-on characteristics. Previous works indicated the statistical distribution of the percolation number, B, for large L (thick varistors) is Gaussian. We used the Monte Carlo computations for thin varistors (L<100). For L<100, histograms of percolation number fit a Lognormal distribution better than a Normal distribution. We realize from the form of the statistical distribution for the percolation number, B, that as P increases, the turn-on will be more rapid. This can be deduced from the low B tail of the statistical distribution. For

small L, the average value of B (percolation number) increases with P, but the minimum value of B, which is L, remains the same.

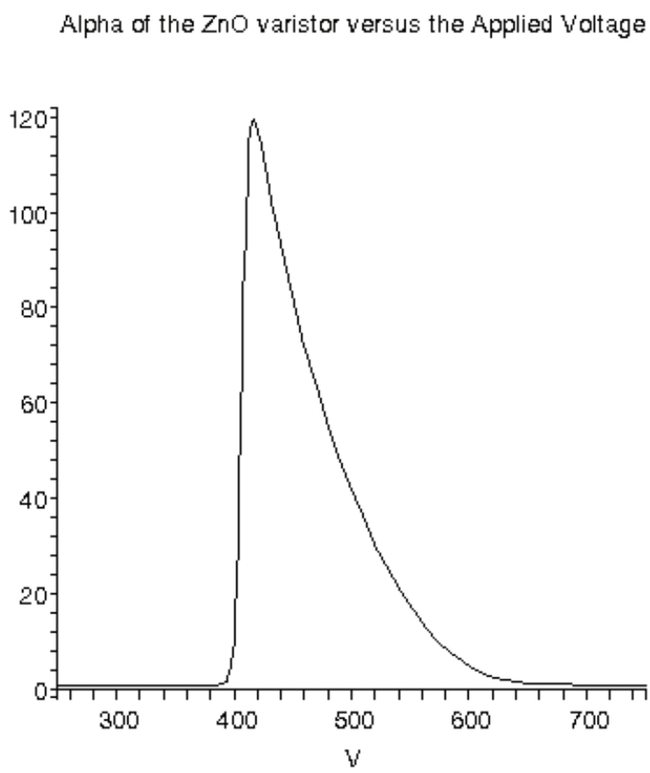

Fig. 20. Variation of α as a function of V for a L=100 (~1 mm thick) varistor.

6. Computer programs

6.1 Basic program for Monte Carlo modeling

```
4   OPEN "D:\Mohammad\B data\L200_1000. K5000. P 0.5\L200_K5000_P0.5.DAT" FOR APPEND
AS #1
'P = Probability of nonconducting grain
5   P = 0.5
'LMAX = Number of the layers across the varistor
6   LMAX = 200
'KMAX = Number of iterations (Current injection to the upper electrode)
7   KMAX = 5000
10  B = 0 : L = 0: K = 0
15  B = 0 : L = 0
20  R = RND(1)
30  IF R > P THEN GOSUB 100
40  IF P >= R AND R > P^5 THEN GOSUB 200
50  IF R <= P^5 THEN GOSUB 300
60  IF L >= LMAX THEN GOSUB 400
70  IF K >= KMAX THEN GOTO 450
80  GOTO 20
```

```
100  B = B + 1
110  L = L + 1
120  RETURN
200  B = B + 1
210  RETURN
300  B = B - 1
310  L = L - 1
320  IF L <= 0 THEN GOTO 15
330  R1 = RND(2)
340  IF R1 > P ^ 4 THEN B = B + 1
350  IF R1 <= P ^ 4 THEN GOTO 300
360  RETURN
400  PRINT #1, B
410  K = K + 1
420  PRINT B, L, K
430  B = 0: L = 0
440  RETURN
450 STOP
500 END
```

6.2 Maple program for varistor's conduction modeling

```
restart;
B:=L*(1+sum(P^n, n=1..infinity)); #  B=The mean number ofactive
grain boundaries through which the current passesbetween
electrodes.
s1:=(log(B) - (1/L)*(log(B))) / (sqrt(L));
s := (((exp(1))^(s1^2))*(((exp(1))^(s1^2))-1))^(1/2);
readlib(log10);
plot3d(s,P=0.1..0.9, L= 10..1000,axes=boxed, title="Standard
Deviation = f(P & L), P=Nonconductivity Probability, L=Number
of varistor grain layers");
J:=10^((tanh(50*log10(VG)-28))*4.5-
5.5)*10^((500*log10(VG)+1000)/450)*10^4;
plot([log10(VG),log10(J),VG=.1..10]);
J1:=subs(VG=VG+.01,J);
alpha_grain := ((log10(evalf(J1)*10^(-2))-log10(evalf(J)*10^(-
2)))/(log10(VG+.01)-log10(VG)),VG=2.8..4.5);
plot(alpha_grain, title="Alpha of a ZnO grain versus Grain
Boundary Voltage");VG:=(V/N);
JJLN:=sum(N*J*(sqrt(s*2*Pi))^(-1)*(exp(-1/2*((log(N)-
B)/sqrt(s))^2)),N=round(B-5*sqrt(s))..round(B+5*sqrt(s)));
L:=20; P:=0.1; JJLN;
JJ1LN:=subs(V=V+1,JJLN);
ALN201:=(log10(evalf(JJ1LN)*10^(-2))-log10(evalf(JJLN)*10^(-
2)))/(log10(V+1)-log10(V));
P; L; plot(ALN201,V=0..1000, title="Alpha LogNormal of the ZnO
varistor versus the Applied Voltage");
B:=L1*(1+sum(P1^n, n=1..infinity));
sn:=B*sum(P1^n,n=1..infinity);readlib(log10);
J:=10^((tanh(50*log10(VG)-28))*4.5-
5.5)*10^((500*log10(VG)+1000)/450)*10^4;
J1:=subs(VG=VG+.01,J);VG:=(V/N); J;
```

```
JJN:=sum(J*(sqrt(sn*2*Pi))^(-1)*(exp(-1/2*((N-
B)/sqrt(sn))^2)),N=round(B5*sqrt(sn))..round(B+5*sqrt(sn)));L1:
=20; P1:=0.1;JJN; JJN1:=subs(V=V+1,JJN);
AN201:=(log10(evalf(JJN1)*10^(-2))-log10(evalf(JJN)*10^(-
2)))/(log10(V+1)-log10(V));
P1; L1; plot(AN201,V=0..1000, title="Alpha of the Normal ZnO
varistor versus the Applied Voltage");
P;L;plot([ALN201,AN201], V=40..120, color=[red ,green ],
style=[line]);
```

7. References

[1] Meshkatoddini, M.R.; Boggs, S.; "Nonlinear Properties of ZnO Ceramics as a Function of Threshold Voltage and Fraction of Non-conducting Grains", Conference Record of ISEI-2006, The 2006 IEEE International Symposium on Electrical Insulation, 11-14 June 2006 Page(s):269 – 272

[2] Andoh H. et al, "Failure mechanisms and recent improvements in ZnO arrester elements," IEEE Electrical Insulation Magazine, vol. 16, no. 1, pp. 25–31, Jan./Feb. 2000. Symposium on Electrical Insulating Materials, Toyohashi, Japan, Sept. 27-30, 1998

[3] Greuter F. & Blatter G., "Electric properties of grain boundaries in polycrystalline compound semiconductors", Semiconductor Science and Technology, vol. 5, pp. 111–137, 1990

[4] Shengtao Li, Jianying Li, Fuyi Liu, M A Alim and G Chen, "The dimensional effect of breakdown field in ZnO varistors", Journal of Applied Physics D, 35, pp.1884-1888, 2002

[5] Tao. M, Bui Ai, Dorlanne O. and Loubiere A., "Different Single Grain Junctions Within a ZnO Varistor", J. Appl. Phys. 61(4), 15 February 1987

[6] Shengtao Li, Feng Xie & Fuyi Liu, "Relation between Residual Voltage Ratio and Micro-structural Parameters of ZnO Varistors", Proceedings of 1998 International Symposium on Electrical Insulating Materials, Toyohashi, Japan, Sept. 27-30, 1998

[7] Robert C.P. and Casella. G., "Monte Carlo Statistical Methods" (second edition). New York: Springer-Verlag, ISBN 0-387-21239-6, 2004

[8] Ueberhuber C.W., Numerical Computation 2: Methods, Software, and Analysis. Berlin: Springer-Verlag, pp. 124-125, 1997

[9] Steven Boggs & Hideyasu Andoh, "A Statistical Approach to Prediction of ZnO Arrester Element Characteristics", IEEE Transactions on Power Delivery, VOL.16, NO. 4, October 2001

[10] H. Andoh, S. Nishiwaki, H. Suzuki, S. Boggs, and J. Kuang, "Failure mechanisms and recent improvements in ZnO arrester elements," IEEE Electrical Insulation Magazine, vol. 16, no. 1, pp. 25–31, Jan./Feb. 2000.Symposium on Electrical Insulating Materials, Toyohashi, Japan, Sept. 27-30, 1998.

[11] M Bartkowiak & G.D.Mahan, "Nonlinear Currents in Voronoi Networks", Physical Review B, Volume 51, Number 16, pp 10825-10831,15 April 1995.

[12] F. Greuter and G. Blatter, "Electric properties of grain boundaries in polycrystalline compound semiconductors", Semiconductor Science and Technology, vol. 5, pp. 111–137, 1990.

[13] Mohammad R. Meshkatoddini & Steven Boggs, " Investigation of the statistical behavior of thin ZnO-based varistors using a Monte Carlo Algorithm", ICEE2006, 14th Iranian Conference on Electrical Engineering, 16-18 May 2006, Tehran, Iran.

[14] M.R.Meshkatoddini et al, "New High Performance ZnO-Based Varistors with Rare-Earth Oxides, for Using in Surge Arresters", PSC 2003, 18th International Power System Conference, Tehran, Iran, 20-22 October 2003.

[15] M.R.Meshkatoddini, "Comparative Study of Different Models for ZnO Varistors", International Conference on Modelling, Simulation and Design of Dielectrics, Institute of Physics, Cambridge, UK, 6-8 April 2005.

[16] D.R.Clarke, "Varistor Ceramics", Journal of American Ceramics Society, 82, 485-502 (1999).

[17] M.Inada, "Effect of Heat-treatment on Crystal Phases, Microstructure and Electrical Properties of Non-ohmic Zinc Oxide Ceramics", Japanese Journal of Applied Physics, 18, 8, 1439-1446 (1979).

[18] J.Kim, T.Kimura, and T.Yamaguchi, "Microstructure Development in Sb2O3-doped ZnO", Journal of Materials Science, 24, 7, 2581-2586 (1989).

[19] T.Senda and R.C.Bradt, "Grain Growth of Zinc Oxide During the Sintering of Zinc Oxide-Antimony Oxide Ceramics", Journal of American Ceramics Society, 74, 6, 1296-1302 (1991).

[20] N.Daneu, A.Recnik, S.Bernik, and D.Kolar, "Microstructural Development in SnO-doped ZnO-Bi2O3 Ceramics", Journal of American Ceramics Society, 83, 12, 3165-3171 (2000).

[21] K.Eda, "Destruction Mechanism of ZnO Varistors Due to High Currents" Journal of Applied Physics, 56, 10, 2948-2955 (1984).

[22] T.K.Gupta, "Application of Zinc Oxide Varistors", Journal of American Ceramics Society, 73, 7, 1817-1840 (1990).

[23] A.Bui, H.T.Nguyen, and A.Loubiere, "High-field ZnO-Based Varistors", Journal of Applied Physics D, 28, 774-782 (1995).

[24] M. Inada, "Formation Mechanism of Non-ohmic Zinc Oxide Ceramics", Japanese Journal of Applied Physics.19, 3, 409-419 (1980).

[25] [25] J.Kim, T.Kimura and T.Yamaguchi, "Sintering of Zinc Oxide Doped with Antimony Oxide and Bismuth Oxide", Journal of American Ceramics Society, 72, 8, 1390-1395 (1989).

[26] S.G.Cho, H.Lee, and S.K.Kim, "Effect of Chromium on the Phase Evaluation and Microstructure of ZnO Doped with Bismuth and Antimony", Journal of Materials Science, 32, 4283-4284 (1997).

[27] M.R.Meshkatoddini, "Measurement of the Potential Barrier Height in ZnO-based Varistors", Proceedings of ICEE2001 Conference, Tehran, Iran, Spring 2001.

[28] M.R.Meshkatoddini, "Impedance Spectroscopy, A New Method for Quality Evaluation of Zinc Oxide Varistors", Proceedings of ICEE1998, Tehran, Iran, Spring 1998.

[29] Nguyen The Hung, "Contribution à l'étude des varistances ZnO à tension de seuil élevée", Thèse de l'Université Paul Sabatier, Toulouse, France, Mars 2002.

[30] Meshkatoddini, M. R., "Investigation of the Influence of the ZnO varistor preparation method on its characteristics", ISEI 2008, Conference Record of the 2008 IEEE International Symposium on Electrical Insulation,Volume , Issue , 9-12 June 2008, Page(s): 320-323, Digital Object Identifier 10.1109/ ELINSL.2008.4570338

[31] Tylor H.F.W., Cement Chemistry, Thomas Telford Publishing, London, pp: 12 – 28. 1997.

[32] Stutzman, P, Scanning Electron Microscopy Imaging Of Hydraulic Cement Microstructure, Cement & Concrete Composites 26: 957– 966. 2004.

[33] Idris, M.S., Kajian Pencirian Mikrostruktur Klinker Semasa Pengeluaran Simen, Unpublished MSc Thesis, School of Materials Engineering, Northern Malaysia University College of Engineering. 2006

[34] Hills, L.M, Clinker Formation and the Value of Microscopy, Proceeding of Twenty-Second International Conference on Cement Microscopy, Montreal, pp: 1 – 12. 2000.

[35] F. Fernandez & R. Diaz, "Metal-Oxide Surge Arrester Model for Fast transient Simulations", IPST-2001, Conference proceedings, 2001.

[36] H.J. Li, S. Birlasekaran & S.S. Choi, "A Parameter Identification Technique for Metal-Oxide Surge Arrester Models", IEEE Transactions on Power Delivery, Vol.17, No.3, July 2002.

[37] C.Talhi, A.Bui, "L'effet de l'oxyde de praséodyme Pr_6O_{11} sur l'augmentation du champ de seuil des varistances à base d'oxyde de zinc", Laboratoire de Génie Électrique de Toulouse 118, route de Narbonne 31062 Toulouse Cedex, ICSD 2004, Toulouse, France.

[38] Renée Legros, André Loubiére, "Etude du vieillissement par la méthode de l'impédance complexe des varistances réalisees par la voie de la chimie douce", LCMI, LGET, Toulouse, France, 1997.

[39] Ramón Puyané1, Isabelle Guy and Renaud Metz, "High Performance Varistor Discs Obtained from Chemically Synthesized Doped Zinc Oxide Powder", Journal of Sol-Gel Science and Technology, Volume 13, Numbers 1-3, pp. 575 – 578, January 1998.

[40] IEEE Working Group 3.4.11 – "Modeling of Metal Oxide Surge Arresters", IEEE Transactions on Power Delivery, Vol.7, No.1, pp. 302-309, January 1992.

[41] A.Bui, C.Talhi, A.Loubière, J.M.Laffargue, "Study of ageing ZnO-based varistor under electrical combined stresses", High Temp. Chem. Proc., 2, 1993, 371-379.

[42] M. Popov, L. van der Sluis, G.C. Paap, and P.H. Schavemaker, "On a hysteresis model for transient analysis," *IEEE Power Eng. Rev.*, vol. 20, pp. 53-54, May 2000.

[43] Daniel W. Durbak, "Surge Arrester Modeling", 0-7803-6672-7/01/$10,00 © IEEE 2001.

[44] R. Diaz, F. Fernandez & J. Silva, "Simulation and Test on Surge Arrester in High-Voltage Laboratory", IPST-2001, Conference proceedings, 2001.

[45] J.Kim, T.Kimura, and T.Yamaguchi, "Microstructure Development in Sb2O3-doped ZnO", Journal of Materials Science, 24, 7, 2581-2586 (1989).

[46] T.Senda and R.C.Bradt, "Grain Growth of Zinc Oxide During the Sintering of Zinc Oxide-Antimony Oxide Ceramics", Journal of American Ceramics Society, 74, 6, 1296-1302 (1991).

[47] N.Daneu, A.Recnik, S.Bernik, and D.Kolar, "Microstructural Development in SnO-doped ZnO-Bi2O3 Ceramics", Journal of American Ceramics Society, 83, 12, 3165-3171 (2000).

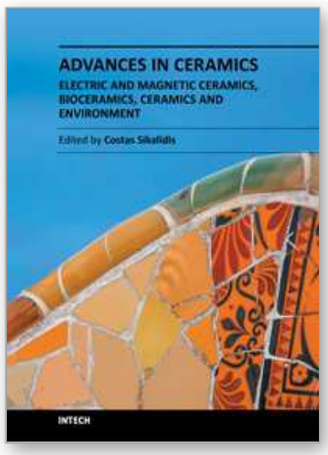

Advances in Ceramics - Electric and Magnetic Ceramics, Bioceramics, Ceramics and Environment

Edited by Prof. Costas Sikalidis

ISBN 978-953-307-350-7
Hard cover, 550 pages
Publisher InTech
Published online 06, September, 2011
Published in print edition September, 2011

The current book consists of twenty-four chapters divided into three sections. Section I includes fourteen chapters in electric and magnetic ceramics which deal with modern specific research on dielectrics and their applications, on nanodielectrics, on piezoceramics, on glass ceramics with para-, anti- or ferro-electric active phases, of varistors ceramics and magnetic ceramics. Section II includes seven chapters in bioceramics which include review information and research results/data on biocompatibility, on medical applications of alumina, zirconia, silicon nitride, ZrO2, bioglass, apatite-wollastonite glass ceramic and b-tri-calcium phosphate. Section III includes three chapters in applications of ceramics in environmental improvement and protection, in water cleaning, in metal bearing wastes stabilization and in utilization of wastes from ceramic industry in concrete and concrete products.

InTech Europe
University Campus STeP Ri
Slavka Krautzeka 83/A
51000 Rijeka, Croatia
Phone: +385 (51) 770 447
Fax: +385 (51) 686 166
www.intechopen.com

InTech China
Unit 405, Office Block, Hotel Equatorial Shanghai
No.65, Yan An Road (West), Shanghai, 200040, China
中国上海市延安西路65号上海国际贵都大饭店办公楼405单元
Phone: +86-21-62489820
Fax: +86-21-62489821

IntechOpen